

# Metadata of the chapter that will be visualized online

---

|                      |  |   |
|----------------------|--|---|
| Chapter Title        | Seismic, Anisotropy                    |   |
| Copyright Year       | 2011                                   |   |
| Copyright Holder     | Springer Science + Business Media B.V. |   |
| Corresponding Author | Family Name                            | <b>Becker</b>   |
|                      | Particle                               |   |
|                      | Given Name                             | <b>Thorsten W.</b>  |
|                      | Suffix                                 |   |
|                      | Division                               | Department of Earth Sciences                                  |
|                      | Organization                           | University of Southern California                             |
|                      | Address                                | 3651 Trousdale Pkwy, MC0740, Los Angeles, CA, 90089-0740, USA |
|                      | Email                                  | thorstinski@gmail.com   |

---

---

# S

1

## 2 SEISMIC, ANISOTROPY

3 Thorsten W. Becker  
 4 University of Southern California, Los Angeles, CA, USA

### 5 Definition

6 Seismic anisotropy refers to the directional dependence of  
 7 seismic wave speeds and particle motion polarizations, as  
 8 well as the splitting of normal modes, as caused by the  
 9 elastic properties of rocks.

### 10 Introduction

11 Many of the minerals that make up Earth are intrinsically  
 12 anisotropic. When rocks are progressively deformed over  
 13 geologic timescales, the alignment of mineral grains  
 14 (lattice-preferred orientation, LPO) can lead to bulk  
 15 anisotropy of the rock. Bulk anisotropy can additionally  
 16 be generated by an ordered assembly of individually iso-  
 17 tropic materials of different wave speeds (shape-preferred  
 18 orientation, SPO). Both types of anisotropy are found  
 19 within the Earth; SPO anisotropy also highlights  
 20 a fundamental ambiguity between isotropic heterogeneity  
 21 and anisotropy. Seismic wave propagation through an  
 22 anisotropic medium depends on the wavelengths over  
 23 which a particular wave type averages, complicating the  
 24 analysis of seismological data. Both LPO and SPO imply  
 25 significantly different (up to ~10%) speeds for waves of  
 26 different polarization or propagation directions, and  
 27 velocity variations can be larger than those expected from  
 28 compositional or thermal heterogeneity. Seismic anisotropy  
 29 is therefore of fundamental importance for structural  
 30 imaging studies. To get robust estimates of the quantities  
 31 of interest for geodynamic interpretation, the trade-off  
 32 between isotropic and anisotropic structure has to be con-  
 33 sidered. Seismic anisotropy provides a powerful link  
 34 between seismic observations and the dynamic processes

that shape the solid Earth, for example, convective flow 35  
 in the case of LPO in the mantle (Figure 1, see Mantle 36  
 Convection). However, anisotropic tomographic inver- 37  
 sions are inherently more nonunique than isotropic imag- 38  
 ing (see Inverse Theory) because a general anisotropic, 39  
 linearly elastic medium has 21 independent components 40  
 of the elasticity tensor, as opposed to 2 in the isotropic 41  
 case. As a consequence of the increased number of param- 42  
 eters and the differences in how data sampling constrains 43  
 isotropic and anisotropic structure, more data are needed 44  
 for the same level of resolution in an anisotropic inversion. 45  
 Typically, additional a priori constraints, such as from 46  
 petrology, are needed to narrow the parameter space. 47  
 These complexities make the study of anisotropy in 48  
 a geodynamic context inherently multidisciplinary, 49  
 involving seismology, mineral physics, rock mechanics, 50  
 and geodynamic modeling. 51

### 52 Basic mathematical description

53 Seismic anisotropy arises when the linear elasticity tensor  
 54  $C$  that connects stress,  $\sigma$ , and strain,  $\epsilon$ , tensors as

$$\sigma_{ij} = \sum_{k=1}^3 \sum_{l=1}^3 C_{ijkl} \epsilon_{kl} \quad (1)$$

55 does not simplify to the isotropic form

$$C_{ijkl} = \lambda \delta_{ij} \delta_{kl} + \mu (\delta_{ik} \delta_{jl} + \delta_{il} \delta_{jk}), \quad (2)$$

56 where  $\lambda$  and  $\mu$  are the first and second (shear modulus)  
 57 Lamé parameters,  $\delta$  the Kronecker delta ( $\delta_{ij} = 1$  for  $i = j$ ,  
 58 and 0 else), and the indices run over the three axes of the  
 59 coordinate system,  $x_1, x_2$ , and  $x_3$ . In general,  $C$  has 81 com-  
 60 ponents, out of which 21 are independent, and the most  
 61 complex (triclinic) form of anisotropy requires the specifi-  
 62 cation of all those components (e.g., Hearmon, 1961; Nye,  
 63 1985; Anderson, 1989). A typical simplification is to

64 assume hexagonal anisotropy, which should capture most  
65 aspects of olivine LPO-related anisotropy in the upper  
66 mantle (Montagner and Anderson, 1989; Browaeyns and  
67 Chevrot, 2004; Becker et al., 2006).

68 If  $C$  is expressed in the  $6 \times 6$  Voigt matrix,  $c$ , notation  
69 where  $c_{mn}$  relates to  $C_{ijkl}$  as  $m = \delta_{ij}i + (1 - \delta_{ij})$   
70  $(9 - i - j)$ , and  $n = \delta_{kl}k + (1 - \delta_{kl})(9 - k - 1)$ , then the  
71 five Love (1927) parameters for the transversely isotropic  
72 medium that results from hexagonal symmetry  
73 correspond to

$$\begin{aligned} A &= c_{11} = \rho v_{\text{PH}}^2, & C &= c_{33} = \rho v_{\text{PV}}^2, \\ L &= c_{44} = \rho v_{\text{SV}}^2, & N &= c_{66} = \rho v_{\text{SH}}^2, \quad \text{and} \\ F &= c_{11}. \end{aligned} \quad (3)$$

74 Here,  $\rho$  is density, and  $v_{\text{PH}}, v_{\text{PV}}$  the velocities for P waves  
75 propagating horizontally (H, in  $x_1$ - $x_2$  plane) and verti-  
76 cally (V,  $x_3$ -axis), respectively. For shear waves,  $v_{\text{SH}}, v_{\text{SV}}$   
77 in Eq. 3 are the velocities for horizontally propagating  
78 waves that are horizontally or vertically polarized, respec-  
79 tively (see Elasticity and Wave Propagation). Transverse  
80 isotropy as a simplified description of material anisotropy  
81 is widely used and developed in exploration seismics (e.g.,  
82 Thomsen, 1986). The top 220 km in the PREM 1D Earth  
83 model (Dziewoński and Anderson, 1981) are also trans-  
84 versely isotropic with vertical symmetry axis as in Eq. 3;  
85 such a medium is said to have bulk radial anisotropy.  
86 (Note that vertically propagating S waves in this case have  
87 the same velocity,  $v_{\text{SV}}$ , regardless of polarization  
88 direction.)

89 Different combinations of the Love parameters or  $c_{nm}$   
90 are used in the literature (e.g., Babuška and Cara, 1991);  
91 for example, anisotropy in PREM is described by two  
92 measures of shear- and compressional-wave anisotropy  
93 strength

$$\xi = \left( \frac{v_{\text{SH}}}{v_{\text{SV}}} \right)^2 = \frac{N}{L} \quad \text{and} \quad \varphi = \left( \frac{v_{\text{PV}}}{v_{\text{PH}}} \right)^2 = \frac{C}{A}, \quad (4)$$

94 respectively, and the parameter  $\eta = F/(A - 2L)$ , which  
95 controls how velocities change between the vertical and  
96 horizontal directions. Another way to characterize the  
97 anisotropy of a transversely isotropic medium is due to  
98 Thomsen (1986), who defined

$$\begin{aligned} \varepsilon &= \frac{c_{11} - c_{33}}{2c_{33}} = \frac{A - C}{C} \quad \text{and} \\ \gamma &= \frac{c_{66} - c_{44}}{2c_{44}} = \frac{N - L}{L} \end{aligned} \quad (5)$$

99 as two different measures of the P and S wave anisotropy  
100 strength, respectively, and a combined parameter

$$\delta^* = \frac{1}{2c_{33}^2} \left[ 2(c_{13} + c_{44})^2 - (c_{33} - c_{44})(c_{11} + c_{33} - 2c_{44}) \right], \quad (6)$$

which, for weak anisotropy, simplifies to

$$\delta = \frac{(c_{13} + c_{44})^2 - (c_{33} - c_{44})^2}{2c_{33}(c_{33} - c_{44})}. \quad (7)$$

The  $\delta$  parameter is important for near-vertical P wave  
propagation and identical to  $\varepsilon$  for “elliptical” anisotropy  
(Thomsen, 1986). Mainprice (2007) provides an account  
of other combinations of  $c_{mn}$  in use to characterize  
a transversely isotropic medium. Those differ, regrettably,  
quite substantially in different fields of study.

If the symmetry axis of the hexagonal anisotropy is in  
the horizontal plane, the anisotropy is termed azimuthal.  
This means that perpendicular fast and slow axes can be  
defined for horizontally propagating SV waves, where  
waves will propagate with  $v_{\text{SV1}} > v_{\text{SV2}}$  along the fast  
and slow orientations, respectively. Any perturbations to  
phase velocity  $p$ ,  $\delta p$ , due to general, but small anisotropy  
can be expressed as a series of isotropic,  $\pi$ -periodic, and  
 $\pi/2$  periodic terms (e.g., Backus, 1965; Forsyth, 1975):

$$\frac{\delta p}{p} \approx A_0 + A_1 \cos(2\Psi) + A_2 \sin(2\Psi) + A_3 \cos(4\Psi) + A_4 \sin(4\Psi). \quad (8)$$

Here,  $\Psi$  is the azimuth of wave propagation, and Eq. 8  
follows from the wave equation and the rank of the elastic-  
ity tensor (Smith and Dahlen, 1973). For mantle rocks, the  
 $2\Psi$  terms are expected to be larger than the  $4\Psi$  contribu-  
tions for Rayleigh waves, which are predominantly sensi-  
tive to SV (Anderson, 1966; Montagner and Nataf, 1986).  
The  $4\Psi$  terms are expected to be bigger than  $2\Psi$  for Love  
waves, motivating the focus on Rayleigh waves for azi-  
muthal anisotropy studies (see Surface Waves).

In general, the wave propagation effects of any elastic-  
ity tensor  $C$  can be analyzed by considering a plane wave  
 $\mathbf{u} = \mathbf{a} \exp(-i\omega(t - \mathbf{s} \cdot \mathbf{x}))$  with  $\omega$  angular frequency, and  $\mathbf{u}$ ,  
 $\mathbf{a}$ ,  $\mathbf{s}$ , and  $\mathbf{x}$  the displacement, polarization, slowness, and  
location vectors, respectively (see Elasticity and Wave  
Propagation).  $\mathbf{s}$  shall have the normalized direction  $\hat{\mathbf{s}}$   
and length of  $1/p$ . Using the momentum equation  $\dot{u}_i = \partial_j \sigma_{ij}$ ,  
Eq. 1, the definition of the strain tensor,  
 $\varepsilon_{ij} = \frac{1}{2}(\partial_i u_j + \partial_j u_i)$ ,  $C$ 's symmetries, and defining  
 $M_{ij} = \frac{1}{\rho} C_{ijkl} \hat{s}_j \hat{s}_l$ , we can write

$$M\mathbf{a} = p^2 \mathbf{a}, \quad (9)$$

which is an eigen problem for the symmetric matrix  $M$ .  
Equation 9 is called the Christoffel equation (e.g.,  
Babuška and Cara, 1991). The eigen vector solutions cor-  
respond to one quasi-P and two quasi-S wave directions,  
and the associated eigen values are the density-velocity  
products  $\rho v_{\text{P}}^2$ ,  $\rho v_{\text{S2}}^2$ , and  $\rho v_{\text{S1}}^2$ . These quantities can be  
contoured for any elasticity tensor, for example as mea-  
sured from single crystals, as a function of incidence angle  
and azimuth, to visualize the anisotropic properties of  
minerals or rocks in isolation (e.g., Mainprice, 2007).  
To generate more realistic synthetic body waves from

147 three-dimensional (3D) variations in anisotropy, semi-  
148 analytical reflectivity methods can be used if anisotropy  
149 is assumed to vary only with depth. However, for the gener-  
150 al case of 3D variations of anisotropy on scales smaller  
151 than a Fresnel zone full, numerical wave propagation solu-  
152 tions are needed.

### 153 Seismological methods

154 Seismic anisotropy can be detected in a number of ways  
155 that can be broadly classified into body- and surface-wave  
156 methods. The split of a shear wave into a fast and slow  
157 polarization direction as discussed for the solutions of  
158 Eq. 9 is akin to optical birefringence; it is exploited by  
159 the most popular method of measuring anisotropy, that uti-  
160 lizing *shear wave splitting* (Ando et al., 1983; Vinnik  
161 et al., 1984; Silver and Chan, 1991). For lithospheric and  
162 mantle applications, one typically considers near-vertical  
163 incidence SKS or SKKS core phases (see Body Waves),  
164 because the effects of any source-side anisotropy are  
165 removed by the S-to-P-to-S conversion upon traversal of  
166 the core. The most common splitting measurement consi-  
167 stitutes of detecting the horizontal orientation of the fast (azi-  
168 muth  $\Psi$ ) pseudo-S wave from recorded particle motions,  
169 as well as determining the delay time  $\delta t$  between the  
170 arrival of the fast and slow  $S$  pulses (e.g., Savage, 1999;  
171 Long and Silver, 2009).

172 Shear wave splitting can be detected using a single  
173 earthquake measured at a single station, if wave propaga-  
174 tion is out of a symmetry axis, and is a unique indicator for  
175 the presence of anisotropy along the ray path. However,  
176 only the highly idealized case of a single, transversely iso-  
177 tropic layer with horizontal symmetry axis can be directly  
178 interpreted in terms of  $\Psi$  and  $\delta t$ . Dipping symmetry axes,  
179 non-hexagonal anisotropy, or variations of anisotropy  
180 with depth will all cause a dependence of apparent split-  
181 ting on back-azimuth (e.g., Schulte-Pelkum and  
182 Blackman, 2003). The nonlinear nature of the splitting  
183 measurement and layer splitting itself can lead to a bias  
184 of sensitivity toward the surface ( $\sim$ one wavelength under  
185 the station), and not simple superposition (e.g., Saltzer  
186 et al., 2000). Such complexities make it imperative to  
187 strive for good back-azimuthal coverage, requiring the  
188 recording of several, suitable earthquakes, which is often  
189 a challenge given station-event geometry, or the duration  
190 of temporary deployments. If back-azimuth variations  
191 are detected, those can be used to make inferences about  
192 the variation of anisotropy with depth, which is undefined  
193 based on isolated measurements where anisotropy could,  
194 in principle, arise anywhere between the core mantle  
195 boundary (CMB) and the surface in the case of SKS split-  
196 ting. If regional S arrivals are used, crossing ray paths can  
197 be used to infer 3D variations of anisotropy (e.g., Abt and  
198 Fischer, 2008). For teleseismic arrivals, the use of sensitiv-  
199 ity kernels (e.g., Chevrot, 2006; Long et al., 2008) for the  
200 multichannel type of measurement of splitting holds great  
201 promise for resolving 3D anisotropy in regions for which  
202 close (closer than Fresnel zone width) station spacing is

available. Broadly speaking, shear wave splitting is, how- 203  
ever, a measurement with good lateral ( $\sim 50$  km), but 204  
fairly poor depth resolution (Savage, 1999). 205

Another single, body-wave arrival method that follows 206  
from Eq. 9 is to use the orientation of the pseudo- $P$  polar- 207  
ization, which may differ by more than  $10^\circ$  from along- 208  
ray, for  $P$  polarization anisotropy (Schulte-Pelkum et al., 209  
2001),  $P_{\text{pol}}$ . A measurement of  $P_{\text{pol}}$  is sensitive to  $\sim$ half 210  
a wavelength underneath the station. If several, near- 211  
horizontal  $P$  paths with different azimuths are available, 212  
as in the case of the refracted  $P_n$  phase, which senses 213  
underneath the Moho, velocities can be plotted against 214  
azimuth to infer azimuthal anisotropy. This method was 215  
used for one of the earliest demonstrations of seismic 216  
anisotropy by Hess (1964), and a global comparison of 217  
 $P_n$  and SKS splitting can be found in Smith and Ekström 218  
(1999). The variations in delay times of teleseismic waves 219  
can also be used directly to infer anisotropy in the mantle 220  
lithosphere (e.g., Babuška et al., 1984; Bokelmann, 2002) 221  
by means of a tomographic inversion (see Earthquake 222  
Tomography), but this method requires knowledge of the 223  
isotropic variations in wave speeds. This is a challenge 224  
for all tomographic approaches to anisotropy because 225  
there will always be a trade-off between isotropic and 226  
anisotropic heterogeneity in the absence of perfect data 227  
coverage (e.g., Tanimoto and Anderson, 1985). In terms 228  
of their depth-sensitivity, the body-wave methods can be 229  
ranked, from shallow to deep, as  $P_n$ ,  $P_{\text{pol}}$ , SKS, and  $P$  230  
delay times (Schulte-Pelkum and Blackman, 2003). 231

At crustal depths, anisotropy can additionally be 232  
detected by wide-angle refraction methods (e.g., Meissner 233  
et al., 2002, 2006). Orthogonal profiling, for example, 234  
may show a mismatch of derived seismic velocities, or 235  
a mismatch of refraction and reflection depths that can 236  
be interpreted in terms of anisotropic wave propagation. 237  
Receiver function methods (e.g., Park and Levin, 2002) 238  
(see Seismic, Receiver Function Technique) yield further 239  
evidence of crustal anisotropy from the existence of split 240  
 $pS$  conversions. Azimuthal variations in radial-transverse 241  
receiver function amplitudes are diagnostic of anisotropy 242  
versus tilted structure, and of the amount of anisotropy 243  
(e.g., Savage, 1998). 244

A wealth of information about anisotropy arises from 245  
the study of *surface waves*. The observation that Love 246  
waves, which mainly sense SH, travel faster than Rayleigh 247  
waves, which mainly sense SV due to their intrinsic polar- 248  
ities, implies the existence of a mean radial anisotropy in 249  
the upper mantle (Anderson, 1966; Dziewoński and 250  
Anderson, 1981). The existence of azimuthal anisotropy 251  
was documented for the Pacific by the study of Rayleigh 252  
waves (Forsyth, 1975), and Nataf et al. (1984) presented 253  
radially anisotropic, upper-mantle tomography. The cur- 254  
rent state of tomographic models for global azimuthal 255  
and radial anisotropy patterns is discussed by Montagner 256  
(2007). Surface wave propagation is dispersive, which 257  
allows the construction of 3D models of anisotropy (see 258  
Seismic Structure of the Earth, Global Models). The most 259  
easily measured phase-velocity period range for 260

261 fundamental modes between  $\sim 50$  and  $150$  s samples from  
262 the lithosphere down to  $\sim 300$  km depth, and Figure 2a  
263 shows azimuthal and radial anisotropy at an astheno-  
264 spheric depth of  $150$  km as well as a global compilation  
265 of SKS splitting results. At the shallow end, array methods  
266 (e.g., Deschamps et al., 2008) and in particular noise  
267 tomography (e.g., Lin et al., 2008) (see Correlation Tech-  
268 niques, Ambient Noise) facilitate extending the period  
269 range to shorter, crustal periods. Overtones can be used  
270 to constrain the deeper mantle, down to the  $660$ -km phase  
271 transition (e.g., Trampert and van Heijst, 2002; Lebedev  
272 and van der Hilst, 2008). Lastly, the long-period surface  
273 wave equivalent of *free oscillations of the Earth* can pro-  
274 vide constraints on the deep Earth, including inner core  
275 anisotropy (e.g., Woodhouse et al., 1986; Tromp, 2001).

276 Surface wave studies of anisotropy have fairly good  
277 depth sensitivity in that they are able to locate the origin  
278 of anisotropic signals in the upper mantle to within  
279  $\sim 100$  km depth. However, particularly compared to body  
280 wave measurements such as SKS splitting, the lateral res-  
281 olution of surface waves is limited, for isotropic structure  
282 to perhaps  $\sim 500$  and  $\sim 50$  km for global and regional  
283 models, respectively, at present. Reasons for discrepancies  
284 between published tomographic models include the differ-  
285 ent treatment of crustal corrections and phase-velocity  
286 measurements, as well as theoretical assumptions about  
287 wave propagation. Perhaps more important factors are  
288 the globally uneven ray path coverage or regularization  
289 choices (see Inverse Theory).

290 A complete, 3D model of general seismic anisotropy  
291 would allow for more powerful petrological and  
292 geodynamic inferences than limited studies that focus  
293 only on a few aspects of anisotropy or wave propagation.  
294 Given the wide array of seismological observations,  
295 a desirable procedure to constrain the full 3D dependence  
296 of anisotropy is to compare different measures of anisotropy  
297 (e.g., Montagner et al., 2000; Wüstefeld et al.,  
298 2009) or to perform a joint inversion (e.g., Montagner  
299 and Nataf, 1988; Šílený and Plomerová, 1996; Marone  
300 and Romanowicz, 2007). Sensitivity kernels that account  
301 for finite-frequency wave-propagation effects and the  
302 resulting complex 3D structure of a measurement's sensi-  
303 tivity to Earth structure (e.g., Chevrot, 2006; Long et al.,  
304 2008; Sieminski et al., 2009) can facilitate the relative  
305 weighting of different observations. Likewise, the incor-  
306 poration of petrological constraints (e.g., Montagner and  
307 Anderson, 1989; Becker et al., 2006) can be used to sim-  
308 plify inversions further (Panning and Nolet, 2008;  
309 Chevrot and Monteiller, 2009).

### 310 Origin of anisotropy

311 The SPO type of anisotropy may be caused by any consis-  
312 tent alignment of entities with different isotropic wave  
313 speeds. Examples include lower crustal lamellae structures,  
314 cracks, or melt inclusions (e.g., Mainprice and Nicholas,  
315 1989; Weiss et al., 1999; Meissner et al., 2006).  
316 Crack alignment will be only important for the shallowest

317 crust where it may be indicative of crustal stress (e.g.,  
318 Crampin and Chastin, 2003). Alignment of partial melt  
319 pockets may play a role both for shallow, extensional litho-  
320 spheric domains, such as underneath mid-oceanic spreading  
321 centers or intracontinental rifts (e.g., Holtzman et al., 2003),  
322 and at the base of the mantle in the Mantle D'' Layer (e.g.,  
323 Moore et al., 2004).

324 In between, the LPO type of anisotropy caused by the  
325 alignment of intrinsically anisotropic crystals is the most  
326 likely cause of anisotropy. The fundamental symmetry  
327 classes of material anisotropy of the constituent minerals  
328 (e.g., Nye, 1985; Anderson, 1989) determine the overall  
329 type of anisotropy in the Earth, and wave propagation  
330 depends critically on the type of anisotropy (e.g., Levin  
331 and Park, 1998; Schulte-Pelkum and Blackman, 2003).  
332 Several crustal rocks show LPO anisotropy; of particular  
333 interest are those rich in phyllosilicates (micas) in the  
334 upper-middle crust, and amphibole minerals in lower crust  
335 (e.g., Christensen and Mooney, 1995). In the upper man-  
336 tle, the highly anisotropic olivine makes up  $\sim 60\%$  of  
337 rocks (e.g., Mainprice, 2007). Laboratory experiments  
338 show that if multi-crystal olivine assemblages are  
339 deformed in the dislocation creep regime, crystals typi-  
340 cally align such that the resulting fast propagation orienta-  
341 tion rotates into the direction of shear, and many mantle  
342 xenoliths show corresponding LPO patterns (Mainprice,  
343 2007; Karato et al., 2008).

344 This connection between rock deformation and  
345 seismic anisotropy allows an association of the patterns  
346 of azimuthal mantle anisotropy (e.g., Figure 2a) with *man-  
347 tle convection* (e.g., McKenzie, 1979; Tanimoto and  
348 Anderson, 1984). A coarse approximation uses tectonic  
349 plate motion to imply deep flow direction, or, more realis-  
350 tically, flow can be calculated from global circulation  
351 models (Hager and O'Connell, 1981). The general associ-  
352 ation between mantle flow and anisotropy in terms of  
353 radial anisotropy is that flow in the upper boundary layer  
354 aligns olivine such that  $v_{SH} > v_{SV}$  underneath oceanic  
355 plates due to a simple shear type of deformation  
356 (Figure 1). In regions of dominantly radial mass transport  
357 such as subduction zones and underneath spreading cen-  
358 ters,  $v_{SV} > v_{SH}$  (Chastel et al., 1993; Montagner, 2007).  
359 The radial and azimuthal anisotropy patterns shown in  
360 Figure 2a are broadly consistent with this expectation  
361 (Figure 2b), though there are also clear differences which  
362 are easier to constrain in regional studies (e.g., Gaherty  
363 et al., 1996). Complexities include variations azimuthal  
364 anisotropy orientations and amplitudes (e.g., Ekström  
365 and Dziewonski, 1998; Smith et al., 2004), and many of  
366 those patterns are accessible to geodynamic modeling,  
367 discussed below.

368 Given the importance of the details of the connection  
369 between seismology and geodynamics, several theoretical  
370 descriptions exist that predict microstructural LPO devel-  
371 opment given general deformation histories, as  
372 constrained by laboratory experiments (e.g., Kaminski  
373 and Ribe, 2001; Blackman, 2007). However, further labo-  
374 ratory constraints, for example on the reorientation of

375 existing LPO fabrics under changing deformation  
376 regimes, are required to decide on the most appropriate  
377 treatment. Complex deformation histories are expected  
378 to lead to complex anisotropy. Yet, under monotonous  
379 deformation (e.g., by simple shear), olivine LPO is  
380 expected to saturate over finite strains of  $\sim 10$ . Amplitude  
381 variations compared to a single crystal may therefore be  
382 mainly due to orientation of the symmetry axis of  
383 the effective elastic tensor for an aggregate of crystals  
384 (cf. Karato et al., 2008).

385 Laboratory work over the last 10 years has further  
386 shown that the role of water content, deviatoric stress  
387 levels, and pressure can lead to significantly different  
388 LPO development from the typical, dry A-type fabrics that  
389 show the “fast axes along flow” alignment discussed  
390 above. For example, the high stress, high water content  
391 B-type fabric aligns the fast axes of olivine orthogonal to  
392 the direction of shear. Variations in water content have  
393 been used to explain some of the variability that is appar-  
394 ent in asthenospheric depth anisotropy, such as the  
395 decrease in azimuthal anisotropy strength across the  
396 Pacific from young to older seafloor, or the variability of  
397 orientations of SKS splitting in subduction zones  
398 (Mainprice, 2007; Karato et al., 2008).

399 LPO development under deformation of mantle rocks  
400 not only affects seismic properties, but also leads to ther-  
401 mal and mechanical anisotropy. The feedback of these  
402 effects into mantle convection and lithospheric deforma-  
403 tion are potentially profound (e.g., Christensen, 1987;  
404 Chastel et al., 1993; Lev and Hager, 2008; Tommasi  
405 et al., 2009) and are currently an active area of research.

## 406 Observations of anisotropy and dynamic 407 inferences

### 408 Whole earth anisotropy

409 Seismic anisotropy is found throughout the Earth, with the  
410 exception of the fluid outer core, though it is concentrated  
411 in certain depth regions (Figure 1). In the mantle, the best-  
412 constrained and strongest signal is found in the uppermost  
413  $\sim 300$  km where SH velocities are faster than SV by up to  
414  $\sim 4\%$  on average, as indicated by the Love–Rayleigh dis-  
415 crepancy. The exact shape of the average radial anisotropy  
416 profile is less certain, though most recent models agree  
417 that the largest anomalies are not found at the surface,  
418 but rather at  $\sim 100$  km depth (Figure 2b). This peak may  
419 be associated with asthenospheric shear flow which is  
420 expected to lead to the largest strain-rates underneath the  
421 oceanic lithosphere, which is up to  $\sim 100$  km thick when  
422 defined thermally (see Mantle Convection). Given that  
423 mantle anisotropy is most likely caused by LPO of olivine,  
424 the peak in seismic anisotropy in the uppermost mantle  
425 has been associated with the relatively high stress and  
426 low temperature depth region where dislocation domi-  
427 nates over diffusion creep (Karato, 1992; Gaherty and  
428 Jordan, 1995) (see Mantle Rheology). Using composite  
429 rheologies, geodynamic models can be used to estimate  
430 the transition depths for the different creep laws, so

delineating the region where LPO forms explicitly (e.g., 431  
McNamara et al., 2002; Podolefsky et al., 2004; Becker 432  
et al., 2008). Once rocks transition into the diffusion-creep 433  
dominated deformation regime, LPO is typically assumed 434  
to be destroyed quickly at high temperatures, or left pre- 435  
served (frozen in) at low temperatures/small velocity gra- 436  
dients. The decrease in radial anisotropy toward the 437  
surface (Figure 2b) may therefore be associated with tec- 438  
tonically older, frozen in structure. On the scales accessi- 439  
ble by surface wave studies, for example, anisotropy in 440  
old lithospheric domains may be less well aligned into 441  
the vertical, or into a coherent horizontal orientation, than 442  
in the asthenosphere, which is shaped by current mantle 443  
convection (e.g., Fouch and Rondenay, 2006). 444

At larger mantle depths, radial anisotropy becomes less 445  
well constrained (e.g., Visser et al., 2008). There is some 446  
indication that radial anomalies pick up around the transi- 447  
tion zone (Figure 1), and several studies have argued for 448  
the existence of azimuthal anisotropy around 660 km 449  
(e.g., Trampert and van Heijst, 2002; Wookey et al., 450  
2002). Most of the lower mantle is nearly isotropic until 451  
the  $D''$  region close to the core mantle boundary where 452  
there is good evidence for the existence of anisotropy from 453  
regional studies (e.g., Moore et al., 2004), and indications 454  
for average radial anisotropy from global studies (Boschi 455  
and Dziewoński, 2000; Panning and Romanowicz, 456  
2006). As for the upper mantle, one may invoke an LPO 457  
reactivation of dislocation creep, for example in 458  
cold, highly deformed subduction slabs (see Figure 1; 459  
McNamara et al., 2002). The other, at present perhaps 460  
equally likely, mechanism that has been invoked for  $D''$  461  
anisotropy is the alignment of melt tubules (SPO). Melt 462  
alignment may also play a role in the transition zone if 463  
the latter represents a melt-rich water filter (Bercovici 464  
and Karato, 2003). The  $D''$  region is expected to be at least 465  
as dynamically complex as the upper thermal boundary 466  
layer, and both domains are affected by compositional 467  
anomalies. Those include the continental lithosphere, with 468  
its stiff, compositionally anomalous and presumably neu- 469  
trally buoyant cratonic keels, and likely piles of dense 470  
material at the base of the mantle in regions displaced 471  
along the CMB from recent subduction (e.g., Garnero, 472  
2004; Garnero and McNamara, 2008). We therefore 473  
expect significant lateral variations in the generation of 474  
anisotropy within  $D''$  depending on the vertical flow set- 475  
ting (Figure 1, e.g., Moore et al., 2004). Close to the 476  
CMB, anisotropy may also vary with depth depending 477  
on if lower mantle material has transitioned to the post- 478  
perovskite phase (e.g., Wookey et al., 2005; Merkel 479  
et al., 2007). 480

There is also robust evidence for anisotropy within the 481  
Earth’s core. Body waves that traverse the inner core and 482  
are aligned with the rotation axis arrive earlier than those 483  
that cross in the equatorial plane (Morelli et al., 1986). 484  
Evidence for anisotropy is also seen in the splitting of nor- 485  
mal modes (Woodhouse et al., 1986), and more recent data 486  
and models for core anisotropy are discussed in Tromp 487  
(2001) and Souriau (2007). However, there are still 488

489 debates on the exact nature of the anisotropy distribution  
490 with depth (cf. Ishii and Dziewoński, 2003). Figure 1  
491 shows radial, shear-wave anisotropy for the inner core  
492 from Beghein and Trampert (2003). This particular model  
493 invoked a hexagonal close-packed phase of iron in the  
494 upper half of the inner core, and perhaps a transition into  
495 a different iron phase at depth, and predicts large ampli-  
496 tudes of radial anisotropy compared to the upper mantle.  
497 The origin of inner core anisotropy is also less clear than  
498 for the upper mantle (Mainprice, 2007). One hypothesis  
499 that has recently been discussed in some detail is freezing  
500 in of convective patterns during the cooling and evolution  
501 of the inner core (Jeanloz and Wenk, 1988; Buffett, 2009;  
502 Deguen and Cardin, 2009).

### 503 Structure and dynamics of the upper boundary layer

504 Seismic anisotropy at every depth range throughout the  
505 Earth holds valuable information on the dynamics of the  
506 planet. The connections can be made quantitative most  
507 easily for the shallower layers where seismological con-  
508 straints abound, rock deformation is accessible via labora-  
509 tory experiments, and geodynamic modeling is fairly well  
510 constrained. In the case of crack anisotropy in the shallow  
511 crust, observations yield constraints on regional stress  
512 fields. Applications include industry work (vertical seis-  
513 mic profiling in boreholes), earthquake studies around  
514 faults, and volcano monitoring where cracking due to  
515 magma migration can be traced.

516 Within the upper convective boundary layer, the oce-  
517 anic plate domains (see Lithosphere, Oceanic) should  
518 most closely resemble the simplified view of radial and  
519 azimuthal anisotropy due to LPO anisotropy formation  
520 in mantle flow as shown in Figure 1. Gaboret et al.  
521 (2003), Becker et al. (2003), and Behn et al. (2004)  
522 showed that mantle circulation from geodynamic models  
523 does indeed provide a valid explanation for azimuthal  
524 anisotropy patterns (Figure 2a), and that comparison of  
525 model predictions with anisotropy can yield constraints  
526 on mantle flow, such as the role of buoyant mantle upwell-  
527 ings as opposed to plate-induced shear. Becker et al.  
528 (2008) provided a quantitative model of radial anisotropy,  
529 and Figure 2b shows the fit of their preferred model to  
530 radial anisotropy averages in the upper mantle, as well as  
531 lateral patterns in azimuthal and radial anisotropy. Results  
532 are consistent with the expectation that the geodynamic  
533 models should describe recent (few 10 s of Myr) astheno-  
534 spheric flow best. The correlations between geodynamics  
535 and the seismological models (Figure 2b) are comparable  
536 or better than the match between different seismological  
537 models. Such first-order agreement between global  
538 geodynamics and seismology motivates current modeling  
539 efforts, for example on constraining the amount of net  
540 rotations of the lithosphere or the degree of lateral viscos-  
541 ity variations (e.g., Becker, 2008; Conrad et al., 2007;  
542 Conrad and Behn, 2010; Kreemer, 2009).

543 Figure 2b shows that geodynamic models typically  
544 underpredict radial anisotropy in the shallower parts of

the lithosphere, which is mainly due to continental 545  
domains. While anisotropy in younger continental litho- 546  
sphere such as in the western USA appears to be well 547  
described by asthenospheric flow, older regions show 548  
more complex behavior such as a consistent orientation 549  
of seismic anisotropy over several hundred kilometers 550  
(e.g., Babuška and Plomerová, 2006). It has been 551  
suggested that anisotropy is concentrated in, and frozen 552  
into, the continental lithosphere, or, alternatively, that 553  
radial anisotropy is largest right underneath the mechani- 554  
cal boundary layer formed by stiff continents (e.g., 555  
Gaherty and Jordan, 1995; Gung et al., 2003; Fouch and 556  
Rondenay, 2006). Figure 3 shows a profile through North 557  
America; anisotropy, as inferred from these models, only 558  
partially conforms to the simplified expectations (cf. 559  
Panning and Romanowicz, 2006). The cross section of 560  
radial anisotropy shows the expected focusing of SH faster 561  
than SV in the Pacific plate, and some regionally enhanced 562  
 $v_{SH} > v_{SV}$  within the eastern USA and the Canadian cra- 563  
ton, but no enhanced anisotropy beneath what would be 564  
inferred to be the base of the continental lithosphere from 565  
the isotropic anomalies. Azimuthal anisotropy is also, 566  
expectedly, strong within the Pacific plate (compare 567  
Figure 2a), but there is an intriguing low-azimuthal anisot- 568  
ropy channel within the eastern North American continen- 569  
tal lithosphere. If such features are due to complex tectonic 570  
deformation with small lateral shear-coherence, or due to 571  
the averaging properties of surface waves and incomplete 572  
ray illumination, remains to be determined. The study of 573  
continental anisotropy is an active area of research, and 574  
many questions such as to the vertical coherence of litho- 575  
spheric deformation and the depth extent of fault zone 576  
localization will benefit from the information that seismic 577  
anisotropy can bring to the table. There are numerous 578  
other, regional tectonic settings where anisotropy can 579  
yield important constraints, and those cannot be compre- 580  
hensively reviewed here. Important examples include contin- 581  
ental transforms and collision zones, spreading centers, 582  
and subduction zones. Reviews of our current understand- 583  
ing of such settings can be found in Silver (1996); Savage 584  
(1999); Park and Levin (2002) and Long and Silver 585  
(2009). 586

587 Powerful dynamic insights notwithstanding, there are 588  
still large uncertainties in every step of the chain of model- 589  
ing that has to be followed. Complexities arise from infer- 590  
ring mantle flow from geodynamics (e.g., role of chemical 591  
vs. thermal buoyancy, uncertainties about rheology), to 592  
predicting LPO textures (e.g., proper microphysical treat- 593  
ment), to inferring elasticity tensors (e.g., homogenization 594  
and temperature/pressure derivatives), to mapping those 595  
tensors in 3D to whatever seismological observable (prefer- 596  
red) or seismological model (more common) are used 597  
to benchmark the models (e.g., finite frequency wave 598  
propagation, sampling). The finding that overall patterns 599  
appear to be well explained (Figure 2), and that synthetic 600  
LPOs match those of xenolith samples provide some 601  
*a posteriori* justification for the modeling rationale. More- 602  
over, these agreements indicate that the bulk of the

603 asthenospheric flow is indeed dominated by dry A-type  
 604 fabrics. However, future refinements of seismological  
 605 imaging, for example through array deployments such as  
 606 EarthScope USArray and temporary seafloor studies, the-  
 607oretical developments in seismology, and the improved  
 608 geodynamic treatment of anisotropy will undoubtedly  
 609 lead to adjustment of our understanding of whole Earth  
 610 anisotropic structure.

## 611 Summary

612 Seismic anisotropy is ubiquitous throughout the Earth and  
 613 provides constraints on dynamic processes, from the stress  
 614 in the crust, the origin and evolution of the continental lith-  
 615-osphere, through convective flow in the upper mantle, to  
 616 core evolution. The state of upper-mantle geodynamic  
 617 modeling is such that important questions, such as about  
 618 absolute plate motion reference frames, intraplate defor-  
 619-mation, or the hydration state of the mantle can be  
 620 addressed. Important issues about the resolution of differ-  
 621-ent seismological datasets and degree of robustness of  
 622 seismological images remain. Joint with the inherent  
 623 uncertainties in geodynamic modeling and how to map  
 624 flow into seismic anisotropy, this means that numerous  
 625 questions for the interpretation of anisotropy observable  
 626 are open. This challenge mandates further theoretical and  
 627 instrumental efforts and that the study of anisotropy  
 628 proceeds interdisciplinary and in a dynamics context.  
 629 Answering those questions holds the promise of arriving  
 630 at a new understanding of the workings of the mantle  
 631 system.

## 632 Acknowledgments

633 Detailed comments by Donna Blackman, Mark Behn, and  
 634 Sergei Lebedev and valuable suggestions from Lapo  
 635 Boschi, Sebastien Chevrot, David Okaya, Mark Panning,  
 636 Vera Schulte-Pelkum, and an anonymous reviewer helped  
 637 improve this contribution.

## 638 Bibliography

639 Abt, D. L., and Fischer, K. M., 2008. Resolving three-dimensional  
 640 anisotropic structure with shear-wave splitting tomography.  
 641 *Geophysical Journal International*, **173**, 859–886.  
 642 Anderson, D. L., 1966. Recent evidence concerning the structure  
 643 and composition of the Earth's mantle. In *Physics and Chemistry*  
 644 *of the Earth*. Oxford: Pergamon, Vol. 6, pp. 1–131.  
 645 Anderson, D. L., 1989. *Theory of the Earth*. Boston, MA: Blackwell  
 646 Scientific Publications (Available online at <http://caltechbook.library.caltech.edu/14/1/TheoryoftheEarth.pdf>, accessed 01/2010).  
 647 Ando, M., Ishikawa, Y., and Yamasaki, F., 1983. Shear-wave polar-  
 648-ization anisotropy in the mantle beneath Honshu, Japan. *Journal*  
 649 *of Geophysical Research*, **88**, 5850–5864.  
 650 Babuška, V., and Cara, M., 1991. *Seismic Anisotropy in the Earth*.  
 651 Dordrecht: Kluwer Academic Publishers.  
 652 Babuška, V., and Plomerová, J., 2006. European mantle lithosphere  
 653 assembled from rigid microplates with inherited seismic

654 anisotropy. *Physics of the Earth and Planetary Interiors*, **158**,  
 655 264–280.  
 656 Babuška, V., Plomerová, J., and Šílený, J., 1984. Spatial variations  
 657 of Presidials and deep structure of the European lithosphere.  
 658 *Geophysical Journal of the Royal Astronomical Society*, **79**,  
 659 363–383.  
 660 Backus, G. E., 1965. Possible forms of seismic anisotropy of the  
 661 uppermost mantle under oceans. *Journal of Geophysical*  
 662 *Research*, **70**, 3429–3439.  
 663 Becker, T. W., 2008. Azimuthal seismic anisotropy constrains net  
 664 rotation of the lithosphere. *Geophysical Research Letters*, **35**,  
 665 L05303, doi:10.1029/2007GL032928, correction: doi:10.1029/  
 666 2008GL033946.  
 667 Becker, T. W., Kellogg, J. B., Ekström, G., and O'Connell, R. J.,  
 668 2003. Comparison of azimuthal seismic anisotropy from surface  
 669 waves and finite-strain from global mantle-circulation models.  
 670 *Geophysical Journal International*, **155**, 696–714.  
 671 Becker, T. W., Chevrot, S., Schulte-Pelkum, V., and Blackman, D. K.,  
 672 2006. Statistical properties of seismic anisotropy predicted by  
 673 upper mantle geodynamic models. *Journal of Geophysical*  
 674 *Research*, **111**, B08309, doi:10.1029/2005JB004095.  
 675 Becker, T. W., Kustowski, B., and Ekström, G., 2008. Radial seis-  
 676-mic anisotropy as a constraint for upper mantle rheology. *Earth*  
 677 *and Planetary Science Letters*, **267**, 213–237.  
 678 Beghein, C., and Trampert, J., 2003. Robust normal mode  
 679 constraints on inner-core anisotropy from model space search.  
 680 *Science*, **299**, 552–555.  
 681 Behn, M. D., Conrad, C. P., and Silver, P. G., 2004. Detection of  
 682 upper mantle flow associated with the African Superplume.  
 683 *Earth and Planetary Science Letters*, **224**, 259–274.  
 684 Bereovici, D., and Karato, S.-i., 2003. Whole-mantle convection and  
 685 the transition-zone water filter. *Nature*, **425**, 39–44.  
 686 Blackman, D., 2007. Use of mineral physics, with geodynamic  
 687 modelling and seismology, to investigate flow in the Earth's  
 688 mantle. *Reports on Progress in Physics*, **70**, 659–689.  
 689 Bokelmann, G. H. R., 2002. Convection-driven motion of the north  
 690 American craton: evidence from P-wave anisotropy. *Geophys-ical*  
 691 *Journal International*, **148**, 278–287.  
 692 Boschi, L., and Dziewoński, A. M., 2000. Whole Earth tomography  
 693 from delay times of P, PcP, PKP phases: lateral heterogeneities in  
 694 the outer core, or radial anisotropy in the mantle? *Journal of*  
 695 *Geophysical Research*, **105**, 25,567–25,594.  
 696 Browaeys, J., and Chevrot, S., 2004. Decomposition of the elastic  
 697 tensor and geophysical applications. *Geophysical Journal Inter-*  
 698 *national*, **159**, 667–678.  
 699 Buffett, B., 2009. Onset and orientation of convection in the inner  
 700 core. *Geophysical Journal International*, **179**, 711–719.  
 701 Chastel, Y. B., Dawson, P. R., Wenk, H.-R., and Bennett, K., 1993.  
 702 Anisotropic convection with implications for the upper mantle.  
 703 *Journal of Geophysical Research*, **98**, 17,757–17,771.  
 704 Chevrot, S., 2006. Finite-frequency vectorial tomography: a new  
 705 method for high-resolution imaging of upper mantle anisotropy.  
 706 *Geophysical Journal International*, **165**, 641–657.  
 707 Chevrot, S., and Monteiller, V., 2009. Principles of vectorial  
 708 tomography – the effects of model parametrization and regulariza-  
 709-tion in tomographic imaging of seismic anisotropy. *Geophysical*  
 710 *Journal International*, **179**, 1726–1736.  
 711 Christensen, N. I., and Mooney, W. D., 1995. Seismic velocity  
 712 structure and composition of the continental crust: a global  
 713 review. *Journal of Geophysical Research*, **100**, 9761–9788.  
 714 Christensen, U. R., 1987. Some geodynamical effects of anisotropic  
 715 viscosity. *Geophysical Journal of the Royal Astronomical*  
 716 *Society*, **91**, 711–736.  
 717 Conrad, C. P., and Behn, M., 2010. Constraints on lithosphere net  
 718 rotation and asthenospheric viscosity from global mantle flow  
 719

- 720 models and seismic anisotropy. *Geochemistry, Geophysics,*  
 721 *Geosystems*, **11**, Q05W05, doi:10.1029/2009GC002970.
- 722 Conrad, C. P., Behn, M. D., and Silver, P. G., 2007. Global mantle  
 723 flow and the development of seismic anisotropy: differences  
 724 between the oceanic and continental upper mantle. *Journal*  
 725 *of Geophysical Research*, **112**, B07317, doi:10.1029/  
 726 2006JB004608.
- 727 Crampin, S., and Chastin, S., 2003. A review of shear wave splitting  
 728 in the crack-critical crust. *Geophysical Journal International*,  
 729 **155**, 221–240.
- 730 Deguen, R., and Cardin, P., 2009. Tectonic history of the Earth's  
 731 inner core preserved in its seismic structure. *Nature Geoscience*,  
 732 **2**, 419–422.
- 733 Deschamps, F., Lebedev, S., Meier, T., and Trampert, J., 2008.  
 734 Azimuthal anisotropy of Rayleigh-wave phase velocities in the  
 735 east-central United States. *Geophysical Journal International*,  
 736 **173**, 827–843.
- 737 Dziewoński, A. M., and Anderson, D. L., 1981. Preliminary refer-  
 738 ence Earth model. *Physics of the Earth and Planetary Interiors*,  
 739 **25**, 297–356.
- 740 Ekström, G., and Dziewoński, A. M., 1998. The unique anisotropy  
 741 of the Pacific upper mantle. *Nature*, **394**, 168–172.
- 742 Forsyth, D. W., 1975. The early structural evolution and anisotropy  
 743 of the oceanic upper mantle. *Geophysical Journal of the Royal*  
 744 *Astronomical Society*, **43**, 103–162.
- 745 Fouch, M., 2006. Upper mantle anisotropy database. Online,  
 746 accessed in 06/2006, [http://geophysics.asu.edu/anisotropy/  
 747 upper/](http://geophysics.asu.edu/anisotropy/upper/).
- 748 Fouch, M. J., and Rondenay, S., 2006. Seismic anisotropy beneath  
 749 stable continental interiors. *Physics of the Earth and Planetary*  
 750 *Interiors*, **158**, 292–320.
- 751 Gaboret, C., Forte, A. M., and Montagner, J.-P., 2003. The unique  
 752 dynamics of the Pacific Hemisphere mantle and its signature  
 753 on seismic anisotropy. *Earth and Planetary Science Letters*,  
 754 **208**, 219–233.
- 755 Gaherty, J. B., and Jordan, T. H., 1995. Lehmann discontinuity as  
 756 the base of an anisotropic layer beneath continents. *Science*,  
 757 **268**, 1468–1471.
- 758 Gaherty, J. B., Jordan, T. H., and Gee, L. S., 1996. Seismic structure  
 759 of the upper mantle in a central Pacific corridor. *Journal of*  
 760 *Geophysical Research*, **101**, 22,291–22,310.
- 761 Garnero, E. J., 2004. A new paradigm for Earth's core-mantle  
 762 boundary. *Science*, **304**, 835–836.
- 763 Garnero, E. J., and McNamara, A. K., 2008. Structure and dynamics  
 764 of the Earth's lower mantle. *Science*, **320**, 626–628.
- 765 Gung, Y., Panning, M., and Romanowicz, B., 2003. Global anisotropy  
 766 and the thickness of continents. *Nature*, **422**, 707–711.
- 767 Hager, B. H., and O'Connell, R. J., 1981. A simple global model of  
 768 plate dynamics and mantle convection. *Journal of Geophysical*  
 769 *Research*, **86**, 4843–4867.
- 770 Hearmon, R. F. S., 1961. *An Introduction to Applied Anisotropic*  
 771 *Elasticity*. London: Oxford University Press.
- 772 Hess, H. H., 1964. Seismic anisotropy of the uppermost mantle  
 773 under oceans. *Nature*, **203**, 629–631.
- 774 Holtzman, B. K., Kohlstedt, D. L., Zimmerman, M. E., Heidelbach,  
 775 F., Hiraga, T., and Hustoft, J., 2003. Melt segregation and strain  
 776 partitioning: implications for seismic anisotropy and mantle  
 777 flow. *Science*, **301**, 1227–1230.
- 778 Ishii, M., and Dziewoński, A. M., 2003. Distinct seismic anisotropy  
 779 at the centre of the earth. *Physics of the Earth and Planetary*  
 780 *Interiors*, **140**, 203–217.
- 781 Jeanloz, R., and Wenk, H. R., 1988. Convection and anisotropy of  
 782 the inner core. *Geophysical Research Letters*, **15**, 72–75.
- 783 Kaminski, É., and Ribe, N. M., 2001. A kinematic model for recryst-  
 784 tallization and texture development in olivine polycrystals.  
 785 *Earth and Planetary Science Letters*, **189**, 253–267.
- Karato, S.-i., 1992. On the Lehmann discontinuity. *Geophysical*  
 786 *Research Letters*, **51**, 2255–2258. 787
- Karato, S.-i., Jung, H., Katayama, I., and Skemer, P., 2008. 788  
 Geodynamic significance of seismic anisotropy of the upper 789  
 mantle: new insights from laboratory studies. *Annual Review of* 790  
*Earth Planetary Sciences*, **36**, 59–95. 791
- Kreemer, C., 2009. Absolute plate motions constrained by shear 792  
 wave splitting orientations with implications for hot spot 793  
 motions and mantle flow. *Journal of Geophysical Research*, 794  
**114**, B10405, doi:10.1029/2009JB006416. 795
- Kustowski, B., Ekström, G., and Dziewoński, A. M., 2008. Aniso- 796  
 tropic shear-wave velocity structure of the Earth's mantle: 797  
 a global model. *Journal of Geophysical Research*, **113**, 798  
 B06306, doi:10.1029/2007JB005169. 799
- Lebedev, S., and van der Hilst, R. D., 2008. Global upper-mantle 800  
 tomography with the automated multimode inversion of surface 801  
 and S-wave forms. *Geophysical Journal International*, **173**, 802  
 505–518. 803
- Lev, E., and Hager, B. H., 2008. Rayleigh Taylor instabilities with 804  
 anisotropic lithospheric viscosity. *Geophysical Journal Interna-* 805  
*tional*, **173**, 806–814. 806
- Levin, V., and Park, J., 1998. *P – SH conversions in layered media* 807  
*with hexagonally symmetric anisotropy: a cookbook.* *Pure and* 808  
*Applied Geophysics*, **151**, 669–697. 809
- Lin, F., Moschetti, M. P., and Ritzwoller, M. H., 2008. Surface wave 810  
 tomography of the western United States from ambient seismic 811  
 noise: Rayleigh and Love wave phase velocity maps. *Geophys-* 812  
*ical Journal International*, **173**, 281–298. 813
- Long, M. D., and Becker, T. W., 2010. Mantle dynamics and seismic 814  
 anisotropy. *Earth and Planetary Science Letters*, **297**, 341–354. 815
- Long, M. D., and Silver, P. G., 2009. Shear wave splitting and 816  
 mantle anisotropy: measurements, interpretations, and new 817  
 directions. *Surveys in Geophysics*, **30**, 407–461. 818
- Long, M. D., de Hoop, M. V., and van der Hilst, R. D., 2008. Wave 819  
 equation shear wave splitting tomography. *Geophysical Journal* 820  
*International*, **172**, 311–330. 821
- Love, A. E. H., 1927. *A Treatise on the Mathematical Theory of* 822  
*Elasticity*. Cambridge: Cambridge University Press. reprinted 823  
 in 1944 by Dover Publications, New York. 824
- Mainprice, D., 2007. Seismic anisotropy of the deep Earth from 825  
 a mineral and rock physics perspective. In Schubert, G., and 826  
 Bercovic, D. (eds.), *Treatise on Geophysics*. Oxford: Elsevier, 827  
 Vol. 2, pp. 437–492. 828
- Mainprice, D., and Nicholas, A., 1989. Development of shape and 829  
 lattice preferred orientations: application to the seismic anisotropy 830  
 of the lower crust. *Journal of Structural Geology*, **11**, 831  
 175–189. 832
- Marone, F., and Romanowicz, F., 2007. The depth distribution of 833  
 azimuthal anisotropy in the continental upper mantle. *Nature*, 834  
**447**, 198–201. 835
- McKenzie, D. P., 1979. Finite deformation during fluid flow. 836  
*Geophysical Journal of the Royal Astronomical Society*, **58**, 837  
 689–715. 838
- McNamara, A. K., van Keken, P. E., and Karato, S.-i., 2002. Devel- 839  
 opment of anisotropic structure in the Earth's lower mantle by 840  
 solid-state convection. *Nature*, **416**, 310–314. 841
- Meissner, R., Mooney, W. D., and Artemieva, I., 2002. Seismic 842  
 anisotropy and mantle creep in young orogens. *Geophysical* 843  
*Journal International*, **149**, 1–14. 844
- Meissner, R., Rabbel, W., and Kern, H., 2006. Seismic lamination 845  
 and anisotropy of the lower continental crust. *Tectonophysics*, 846  
**416**, 81–99. 847
- Merkel, S., McNamara, A. K., Kubo, A., Speziale, S., Miyagi, L., 848  
 Meng, Y., Duffy, T. S., and Wenk, H.-R., 2007. Deformation of 849  
 (Mg, Fe)SiO<sub>3</sub> post-perovskite and D<sup>h</sup> anisotropy. *Science*, 850  
**316**(5832), 1729–32. 851

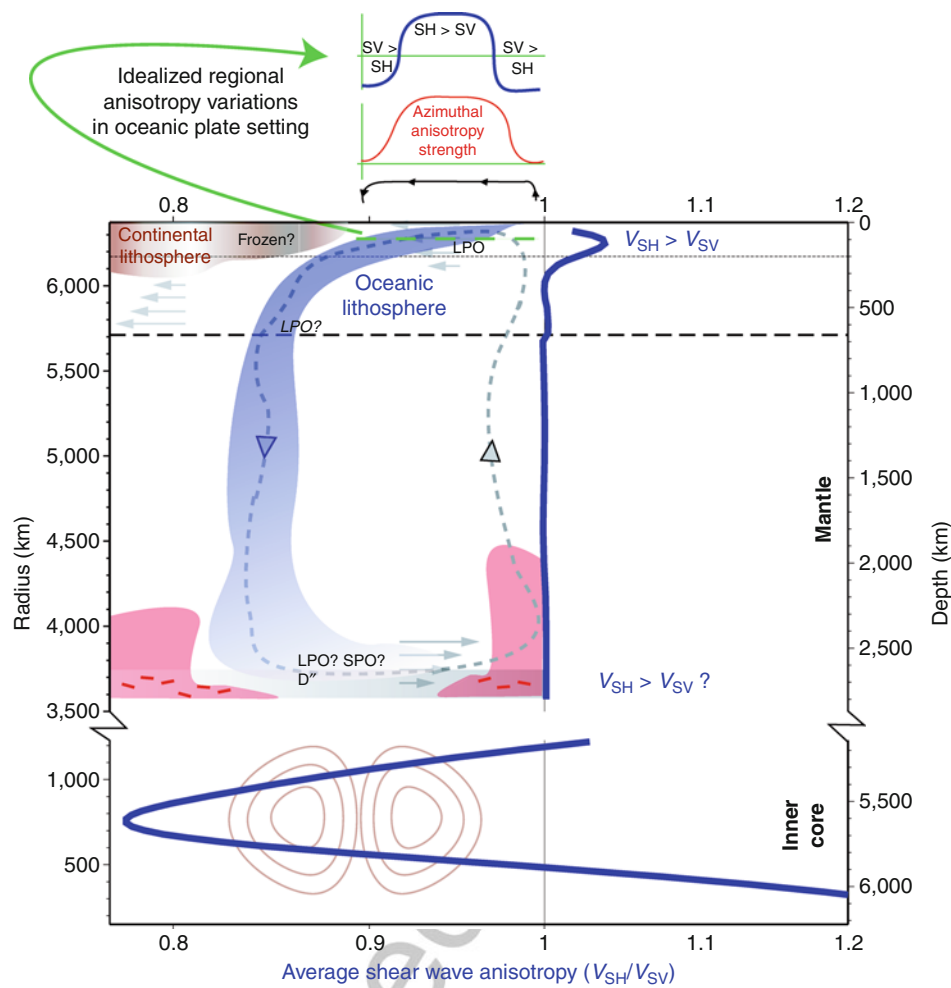
- 852 Montagner, J.-P., 2007. Upper mantle structure: Global isotropic  
 853 and anisotropic elastic tomography. In Schubert, G., and  
 854 Bercovici, D. (eds.), *Treatise on Geophysics*. Amsterdam:  
 855 Elsevier, Vol. 1, pp. 559–589.
- 856 Montagner, J. P., and Anderson, D. L., 1989. Petrological con-  
 857 straints on seismic anisotropy. *Physics of the Earth and Plane-  
 858 tary Interiors*, **54**, 82–105.
- 859 Montagner, J.-P., and Nataf, H.-C., 1986. A simple method for  
 860 inverting the azimuthal anisotropy of surface waves. *Journal of  
 861 Geophysical Research*, **91**, 511–520.
- 862 Montagner, J. P., and Nataf, H. C., 1988. Vectorial tomography-I.  
 863 Theory. *Geophysical Journal*, **94**, 295–307.
- 864 Montagner, J.-P., Griot-Pommera, D.-A., and Lave , J., 2000. How  
 865 to relate body wave and surface wave anisotropy? *Journal of  
 866 Geophysical Research*, **105**, 19,015–19,027.
- 867 Moore, M. M., Garnero, E. J., Lay, T., and Williams, Q., 2004. Shear  
 868 wave splitting and waveform complexity for lowermost mantle  
 869 structures with low-velocity lamellae and transverse isotropy.  
 870 *Journal of Geophysical Research*, **103**, B02319, doi:10.1029/  
 871 2003JB002546.
- 872 Morelli, A., Dziewonski, A. M., and Woodhouse, J. H., 1986.  
 873 Anisotropy of the inner core inferred from PKIKP travel times.  
 874 *Geophysical Research Letters*, **13**, 1545–1548.
- 875 Nataf, H.-C., Nakanishi, I., and Anderson, D. L., 1984. Anisotropy  
 876 and shear velocity heterogeneity in the upper mantle. *Geophysi-  
 877 cal Research Letters*, **11**, 109–112.
- 878 Nye, J. F., 1985. *Physical Properties of Crystals*. London: Oxford  
 879 University Press.
- 880 Panning, M., and Romanowicz, B., 2006. A three-dimensional radi-  
 881 ally anisotropic model of shear velocity in the whole mantle.  
 882 *Geophysical Journal International*, **167**, 361–379.
- 883 Panning, M. P., and Nolet, G., 2008. Surface wave tomography for  
 884 azimuthal anisotropy in a strongly reduced parameter space.  
 885 *Geophysical Journal International*, **174**, 629–648.
- 886 Park, J., and Levin, V., 2002. Seismic anisotropy: tracing plate  
 887 dynamics in the mantle. *Science*, **296**, 485–489.
- 888 Podolefsky, N. S., Zhong, S., and McNamara, A. K., 2004. The  
 889 anisotropic and rheological structure of the oceanic upper mantle  
 890 from a simple model of plate shear. *Geophysical Journal Inter-  
 891 national*, **158**, 287–296.
- 892 Saltzer, R. L., Gaherty, J. B., and Jordan, T. H., 2000. How are ver-  
 893 tical shear wave splitting measurements affected by variations in  
 894 the orientation of azimuthal anisotropy with depth? *Geophysical  
 895 Journal International*, **141**, 374–390.
- 896 Savage, M., 1998. Lower crustal anisotropy or dipping boundaries?  
 897 Effects on receiver functions and a case study in New Zealand.  
 898 *Journal of Geophysical Research*, **103**, 15,069–15,087.
- 899 Savage, M. K., 1999. Seismic anisotropy and mantle deformation:  
 900 what have we learned from shear wave splitting? *Reviews of  
 901 Geophysics*, **37**, 65–106.
- 902 Schulte-Pelkum, V., and Blackman, D. K., 2003. A synthesis of  
 903 seismic *P* and *S* anisotropy. *Geophysical Journal International*,  
 904 **154**, 166–178.
- 905 Schulte-Pelkum, V., Masters, G., and Shearer, P. M., 2001. Upper  
 906 mantle anisotropy from long-period *P* polarization. *Journal of  
 907 Geophysical Research*, **106**, 21,917–21,934.
- 908 Sieminski, A., Trampert, J., and Tromp, J., 2009. Principal compo-  
 909 nent analysis of anisotropic finite-frequency sensitivity kernels.  
 910 *Geophysical Journal International*, **179**, 1186–1198.
- 911  ileny, J., and Plomerov, J., 1996. Inversion of shear-wave split-  
 912 ting parameters to retrieve three-dimensional orientation of  
 913 anisotropy in continental lithosphere. *Physics of the Earth and  
 914 Planetary Interiors*, **95**, 277–292.
- 915 Silver, P. G., 1996. Seismic anisotropy beneath the continents:  
 916 probing the depths of geology. *Annual Review of Earth Plane-  
 917 tary Sciences*, **24**, 385–432.
- Silver, P. G., and Chan, W. W., 1991. Shear wave splitting and sub-  
 continental mantle deformation. *Journal of Geophysical  
 Research*, **96**, 16,429–16,454.
- Smith, D. B., Ritzwoller, M. H., and Shapiro, N. M., 2004. Stratifi-  
 cation of anisotropy in the Pacific upper mantle. *Journal of Geo-  
 physical Research*, **109**, B11309, doi:10.1029/2004JB003200.
- Smith, G. P., and Ekstr m, G., 1999. A global study of  $P_n$  anisotropy  
 beneath continents. *Journal of Geophysical Research*, **104**,  
 963–980.
- Smith, M. L., and Dahlen, F. A., 1973. The azimuthal dependence of  
 Love and Rayleigh wave propagation in a slightly anisotropic  
 medium. *Journal of Geophysical Research*, **78**, 3321–3333.
- Souriau, A., 2007. The Earth’s core. In Romanowicz, B., and  
 Dziewonski, A. (eds.), *Treatise on Geophysics*. Amsterdam:  
 Elsevier, Vol. 1, pp. 655–693.
- Tanimoto, T., and Anderson, D. L., 1984. Mapping convection in  
 the mantle. *Geophysical Research Letters*, **11**, 287–290.
- Tanimoto, T., and Anderson, D. L., 1985. Lateral heterogeneity and  
 azimuthal anisotropy of the upper mantle: Love and Rayleigh  
 waves 100–250 s. *Journal of Geophysical Research*, **90**,  
 1842–1858.
- Thomsen, L., 1986. Weak elastic anisotropy. *Geophysics*, **51**, 1954–  
 1966.
- Tommasi, A., Knoll, M., Vauchez, A., Sgnorelli, J., Thoraval, C.,  
 and Loge, R., 2009. Structural reactivation in plate tectonics con-  
 trolled by olivine crystals anisotropy. *Nature Geosciences*, **2**,  
 423–427.
- Trampert, J., and van Heijst, H. J., 2002. Global azimuthal anisot-  
 ropy in the transition zone. *Science*, **296**, 1297–1299.
- Tromp, J., 2001. Inner core anisotropy and rotation. *Annual Review  
 of Earth and Planetary Sciences*, **29**, 47–69.
- Vinnik, L., Kosarev, G. L., and Makeyeva, L. I., 1984. Anisotropy  
 of the lithosphere from the observations of *SKS* and *SKKS*  
 phases. *Proceedings of Academic Sciences USSR*, **278**, 1335–  
 1339.
- Visser, K., Trampert, J., Lebedev, S., and Kennett, B. L. N., 2008.  
 Probability of radial anisotropy in the deep mantle. *Earth and  
 Planetary Science Letters*, **270**, 241–250.
- Weiss, T., Siegesmund, S., Rabbel, W., Bohlen, T., and Pohl, M.,  
 1999. Seismic velocities and anisotropy of the lower continental  
 crust: a review. *Pure and Applied Geophysics*, **156**, 97–122.
- Woodhouse, J. H., Giardini, D., and Li, X.-D., 1986. Evidence for  
 inner core anisotropy from free oscillations. *Geophysical  
 Research Letters*, **13**, 1549–1552.
- Wookey, J., Kendall, J.-M., and Barruol, G., 2002. Mid-mantle  
 deformation inferred from seismic anisotropy. *Nature*, **415**,  
 777–780.
- Wookey, J., Stackhouse, S., Kendall, J.-M., Brodholt, J., and Price,  
 G. D., 2005. Efficacy of the post-perovskite phase as an explana-  
 tion for lowermost-mantle seismic properties. *Nature*, **438**,  
 1004–1007.
- W stefeld, A., Bokelmann, G. H. R., Barruol, G., and Montagner,  
 J. P., 2009. Identifying global seismic anisotropy patterns by cor-  
 relating shear-wave splitting and surface-wave data. *Physics of  
 the Earth and Planetary Interiors*, **176**, 198–212.

**Cross-references**

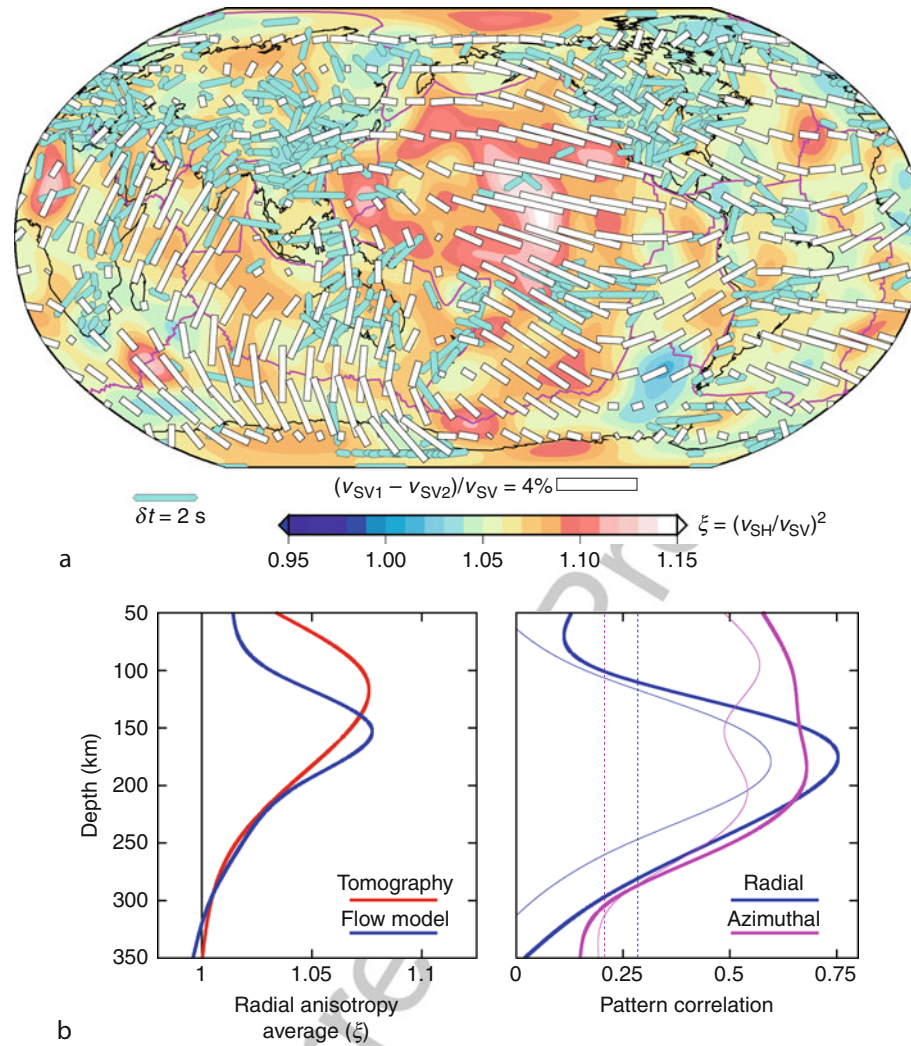
- Body Waves 974  
 Correlation Techniques, Ambient Noise 975  
 Earthquake Tomography 976  
 Elasticity and Wave Propagation 977  
 Free Oscillations of the Earth 978  
 Inverse Theory 979  
 Lithosphere, Continental 980  
 Lithosphere, Oceanic 981

|     |                                      |   |     |
|-----|--------------------------------------|---|-----|
| 982 | Mantle Convection                    | Seismic Structure of the Earth, Global Models | 986 |
| 983 | Mantle D'' Layer                     | Shear Wave Splitting                          | 987 |
| 984 | Mantle Rheology                      | Surface Waves                                 | 988 |
| 985 | Seismic, Receiver Function Technique |   |     |

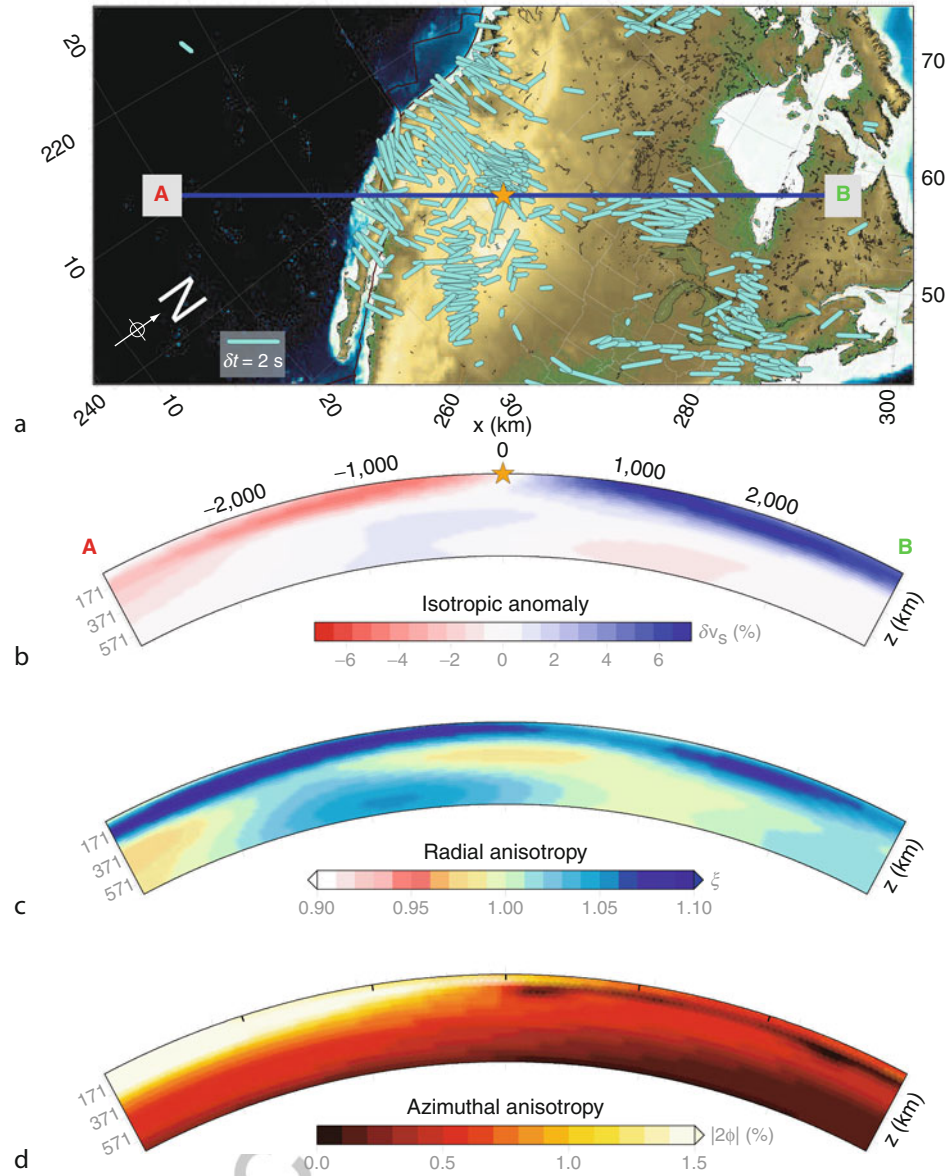
Uncorrected Proof



**Seismic, Anisotropy, Figure 1** Cartoon of the possible distribution of whole Earth anisotropy (note scale break at CMB) with geodynamic interpretation (cf. Montagner, 2007); dotted and dashed horizontal lines indicate 200 and 660 km depths, respectively. The heavy blue lines in center show average radial anisotropy from Kustowski et al. (2008) for the mantle and from Beghein and Trampert (2003) for the inner core. Underneath oceanic plates, mantle flow is primarily horizontal, leading to LPO anisotropy alignment with  $v_{SH} > v_{SV}$ , while the radial mass transport associated with upwellings and downwellings may lead locally  $v_{SV} > v_{SH}$ . Beneath continental regions, both frozen in anisotropy from past tectonic deformation and asthenospheric anisotropy from present-day convection may contribute. The gray, dashed, circular line in the mantle indicates an idealized flow trajectory for a downwelling slab (blue) displacing a thermochemical "pile" (red) at the core mantle boundary (cf. Garnero and McNamara, 2008). This deep flow may affect CMB dynamics and lead to LPO and/or SPO anisotropy (Modified from Long and Becker, 2010).



**Seismic, Anisotropy, Figure 2** Global, uppermost mantle seismic anisotropy. (a) Seismological constraints: Radial (background, from Kustowski et al., 2008) and azimuthal anisotropy (white sticks indicating fast orientation, from Lebedev and van der Hilst, 2008) at 150 km, as well as SKS splitting (cyan sticks). SKS data are shown as a simple  $5^\circ$  average of the compilations by Fouch (2006) and Wüstefeld et al. (2009), but note that such averaging only provides a simplified view of azimuthal anisotropy (see text, and Schulte-Pelkum and Blackman, 2003, for example). (b) Radial anisotropy layer averages, on left, for the seismological model of Kustowski et al. (2008) and as predicted from the best-fitting geodynamic model of Becker et al. (2008). On right, pattern correlations up to spherical harmonic degree 8 between the same geodynamic model and radial (from Kustowski et al., 2008) and azimuthal (from Lebedev and van der Hilst, 2008) seismic tomography. *Heavy* and *thin lines* denote oceanic lithosphere only and global correlations, respectively. *Vertical, dashed lines* show 95% significance level (Modified from Long and Becker, 2010).



**Seismic, Anisotropy, Figure 3** Pacific and North American upper mantle anisotropy. (a) SKS splitting (as in Figure 2, but averaged by  $0.5^\circ$ ) and location of cross-continent profile; (b) isotropic shear wave velocity relative to background (Voigt average, from Kustowski et al., 2008); (c) radial anisotropy ( $\xi = (v_{SH}/v_{SV})^2$ , from Kustowski et al., 2008); and (d) strength of azimuthal anisotropy ( $|(v_{SV1} - v_{SV2})/v_{SV}|$ , from Lebedev and van der Hilst, 2008). (Modified from Long and Becker, 2010.)